15TH IEA HEAT PUMP CONFERENCE
MAY 26–29, 2026 | HOFBURG
VIENNA 2026
DECARBONISATION THROUGH INNOVATION

Experimental and visualization study on compact microchannel condenser with header-orifice liquid-vapor separator

Shijie XU[a], Yiming LI[a], Bin SUN[b], Guoqing WANG[b], Yinghui SHI[b], Suxin QIAN*[a], Jianlin YU[a]

[a]Institute of Refrigeration and Cryogenic, Xi'an Jiaotong University;
Xi'an, Shaanxi, 710049, China
[b]Hisense Refrigerator Co., Ltd.
Tsingtao, Shandong, 266104, China

Abstract

Liquid-vapor separation enhances heat transfer and reduces pressure drop by optimizing refrigerant phase distribution. This technique has been implemented in parallel flow condensers in a simple and cost-effective manner by drilling orifices in the baffles. However, its performance under lower heat load conditions, relevant to compact heat pump system, has not been sufficiently studied, hindering its application in this industry. In this study, a series of microchannel parallel flow condensers with varied orifice positions were fabricated for thermohydraulic experiments. Several units were equipped with observation windows for flow visualization. Isobutane (R600a) was employed as the working fluid, with mass flow rates of 0.3 g/s and 0.5 g/s. The results demonstrate that the orificed baffle structure performs effectively when adequate liquid accumulates over it. The header-orifice condensers achieved an average pressure drop reduction of 0.43 kPa compared to the baseline, while maintaining nearly invariant subcooling degrees. Flow visualization confirmed the advantage of the tube-side orifice position in promoting liquid accumulation over other positions, thereby reducing gas entrainment into the subsequent condenser pass. This work provides practical guidance for applying header-orifice liquid-vapor separators in parallel flow microchannel condensers for low-heat-load applications.

Keywords: Heat pump,Microchannel condenser , Heat transfer enhancement, Liquid separation, Visualization, Isobutane.

1. Introduction

Heat exchanger optimization plays a critical role in enhancing the performance of refrigeration and heat pump systems [1]. Such optimization is typically categorized into active and passive methods, with passive approaches being more widely adopted due to their economic feasibility and operational simplicity. Passive methods include surface modification, fluid additives, engineered fin geometries, and phase-separation mechanisms. Among these, the gravity-driven liquid-vapor separation technique has emerged as particularly promising owing to its straightforward implementation. One of the earliest implementations was developed by Oh et al. for a parallel flow condenser with a dual-chamber header [2]. In this design, one chamber acted as a T-junction liquid-vapor separator while the other functioned as a liquid receiver. Upon refrigerant entry into the T-junction chamber, vapor rose upward and liquid drained downward due to gravity. The vapor was then condensed in subsequent passes and collected in the receiver chamber with the condensate. A similar dual-chamber header was implemented in an automotive condenser for quantitative analysis and flow visualization [3]. Their study revealed that inlet quality exerted minimal impact on separation efficiency under high mass flow rates. Further system-level investigation on a mobile air conditioner [4] demonstrated that the system using a liquid-vapor separation condenser (LSC) achieved up to 6.6% higher COP than the baseline system with a conventional condenser. Li and Hrnjak further investigated the separation mechanisms of R134a at low vapor qualities in LSCs [5]. They found that the separation efficiency decreased significantly when liquid entered the vapor exit, due to excessive liquid loading and high upward vapor velocity. Their work provided a valuable reference for the engineering application of this technique.

Beyond the dual-chamber T-junction-like design, another scheme offered a more straightforward implementation. Wu et al. first proposed this technique, which involves drilling holes in the in-header baffles of a conventional parallel flow condenser (hereinafter referred to as HLSC to distinguish it from the conventional LSC) [6]. Under gravity, condensate accumulated on the orifice baffles and flowed into subsequent passes, thereby preventing gaseous refrigerant from passing through. This technique was first applied in an air-cooled condenser, achieving similar or even better heat transfer performance with a 37% reduction in heat transfer area. Following this, other researchers conducted extensive studies on HLSC. For instance, Chen et al. applied it to a split-type air conditioner, achieving comparable cooling capacity and Energy Efficiency Ratio (EER) while reducing the heat transfer area by 36.9% and refrigerant charge by 19.7% [7]. A subsequent study confirmed consistent performance across varying ambient temperatures, with maximum reductions of 67% in heat transfer area and 80% in refrigerant charge, while maintaining the same cooling capacity and EER as the baseline system [8]. Zhong et al. compared an HLSC with a conventional condenser over wider ranges of mass flux (450–770 kg/(m²·s)), heat flux (1.5–2.45 kW/m²), and condensing temperature (45–50 ° C). Their work quantified the conditions under which the HLSC outperforms the conventional condenser [9]. Another study by Chen et al. extended HLSC application to both heating and cooling modes in a split-type air conditioner, reporting COP and EER improvements of 7.8% and 9.8%, respectively [10]. In addition to experimental work, numerical studies on HLSC have also been performed. Hua et al. developed an HLSC model based on genetic algorithm and segment self-subdivision, with prediction deviations within ±20% of experimental data (Hua et al., 2019). Luo et al. incorporated an HLSC into an organic Rankine cycle (ORC) system using a zeotropic fluid. Their numerical case study showed a 17.6% reduction in heat transfer area and specific investment cost savings of 13.3–18.4% compared to a conventional unit [11]. While HLSC has proven effective in these applications, its miniaturization for smaller systems, which hold significant potential for economic and energy savings, remains challenging.

There are about three hundred thousand convenience stores are operating worldwide of the top four retail brands[12]. Therefore, a prime underlying application of such smaller systems is regarded as substitutions of electric hot food warmer display cases in convenience store, which can reduce hundreds of thousands of tons' carbon emissions per year. And the HLSC is definitely one of the prospective and alternative techniques to enhance the performance of these small system. However, the results from previous studies are likely not directly applicable, as the flow characteristics at such low mass flow rates differ significantly from those at higher mass flow rates.

This study investigated a series of microchannel parallel flow HLSCs using R600a. Several units were fabricated with observation windows to visualize the fluid flow characteristics associated with the drilled orifices. In addition, the thermohydraulic performance of the condensers was evaluated. The study aims to elucidate the flow mechanisms of R600a within these HLSCs and to provide guidance for practical applications.

2. Condenser configuration and experimental setup

2.1. Studied Microchannel Parallel Condenser Configuration

This study fabricated two HLSC variants, primarily distinguished by orifice diameter and channel geometry. These designs correspond to two representative operating conditions, characterized by significantly different levels of liquid accumulation above the orificed baffles. The first variant used smooth microchannel tubes with a 1.0 mm orifice on the second baffle, whereas the second employed inner-grooved tubes with a 0.6 mm orifice on the same baffle. All other geometrical parameters were identical. Both designs featured four parallel flow passes with an identical tube arrangement of 7, 4, 3, and 3 tubes per pass (Figure 1, left). In accordance with this pass arrangement, all condensers incorporated three baffles, with the orifices fixed at specific locations on the second baffle. The possible orifice locations, presented in Figure 1 (right), included three positions: tube-side (A), central (B), and header-side (C), where the distance x was equal to one quarter of the header's inner radius.

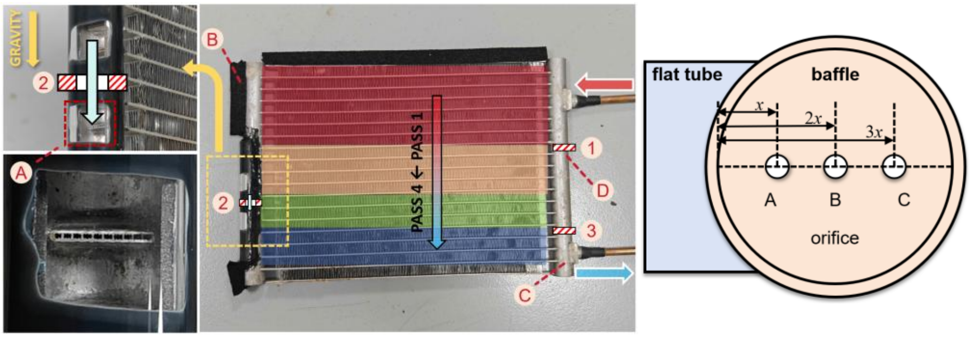

Figure 1: One of the studied condensers with observation windows (left subfigure, 1-3: baffle sequence, 2: baffle with the orifice, A: observation window, B: foam gasket, C: aluminum header, D: baffle) and orifice locations (right subfigure, A: orifice position 1, named tube-side orifice, B: orifice position 2, named central orifice, C: orifice position 3, named header-side orifice).

2.2. Experimental Setup

Isobutane (R600a) was selected as the refrigerant due to its prevalent use in domestic refrigerators. The condensers were evaluated on a heat exchanger test rig housed in an environmental chamber. The test rig comprised two computer-controlled subsystems: (1) the refrigerant flow regulation system (Figure 2, left) and (2) the airflow regulation system (Figure 2, right). These subsystems were used to regulate the boundary conditions of the tested heat exchangers. During testing, the condensing pressure, evaporating pressure, and superheat degree were regulated primarily by the accumulator and the heat exchangers, respectively, both of which were equipped with electric heaters. The refrigerant flow was regulated by a high-precision electronic expansion valve. An auxiliary condenser was installed in series downstream of the tested condenser to ensure an adequate subcooling degree, thereby maintaining a stable refrigerant mass flow rate. In the airflow regulation system, an air tunnel was connected in series to the downstream section of an air duct. A centrifugal fan was installed at the downstream end of the air tunnel for airflow rate regulation. The airflow rate was measured with a nozzle flowmeter mounted inside the air tunnel. The tested condensers were positioned in the mid-section of the air duct, with thermocouples installed at both the inlet and outlet to measure the temperature. Figure 3 provides a detailed view of the airflow duct, which exhibits a double-layered structure consisting of a smaller handmade inner air duct nested within a larger outer one. The smaller inner air duct was sealed with polyurethane rigid foam sheets to accommodate the tested condensers. A segment of the sheet near the observation window was replaced with a transparent acrylic plate. An industrial CCD camera was positioned nearby to capture images and videos of the refrigerant flow. The camera position, condensing pressure, and superheat degree at the condenser inlet were adjusted in accordance with the experimental plan. Data collection began only after the signal curves had remained stable for at least 10 minutes and then continued for a further 10 minutes. The sampling frequency was maintained at 1 Hz throughout the sampling period. Finally, the collected data were averaged over the entire sampling period.

The ambient conditions in the climate chamber were maintained at 32°C and 55% relative humidity. The condensers were operated under two sets of conditions: mass flow rates of 0.3 g/s and 0.5 g/s, at corresponding condensing pressures of 530 kPa and 560 kPa, respectively. The inlet superheat of the condensers was maintained at 5 K. To ensure sufficient liquid sealing at the orifice, the operating pressure for the inner-grooved tube condenser operating at 0.5 g/s was increased to 590 kPa, which resulted in a larger heat transfer temperature difference. The specifications and measurement uncertainties of all temperature and pressure sensors used in this study are detailed in Table 1.

Table 1. Temperature and pressure sensors in experiment.

Sensor type	Position	Model	Measurement range	Uncertainty
pressure	inlet/outlet of the condenser (ref.)	Unik5000	0-1500 kPa(A)	0.04% FS
differential pressure	on both sides of the nozzle	EJA120A	0-1000 Pa	±0.2%
temperature	inlet/outlet of the condenser (ref.)	PT-100 (AAA Class)	-60-160°C	±0.05 K
temperature	inlet/outlet of the condenser (air)	TT-T-24	-200-200°C	±0.5 K
relative humidity	-	HC2-S(3)H	0-100% RH	±0.5%

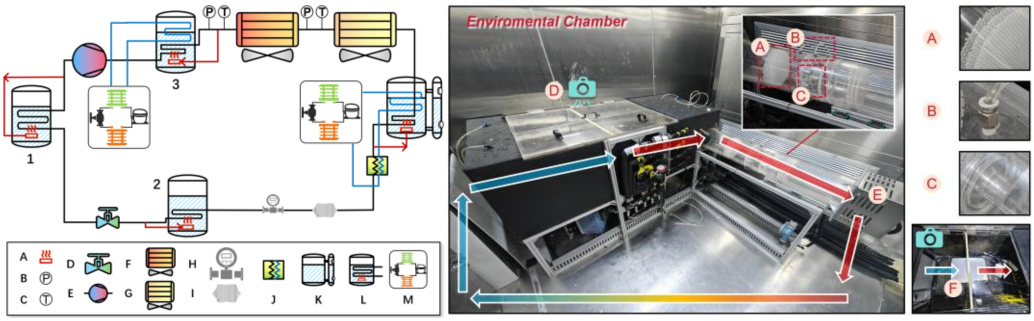

Figure 2: Experimental rig: schematic diagram (left subfigure, A: electric heater, B: pressure transducer, C: temperature sensor, D: electronic expansion valve, E: compressor, F: tested condenser; G: auxiliary condenser, H: mass flow meter, I: dry filter, J: sub-cooler, K: accumulator, L: heat exchanger equipped with adjustable power electric heater, M: auxiliary chiller.) and photo (right subfigure, A: honeycomb flow straightener, B: differential pressure tap, C: nozzle, A, B and C construct the nozzle flowmeter, D: the tested condenser section, E: an adjustable speed centrifugal fan, F: the air duct was made of polyurethane sheets to contain condensers.)

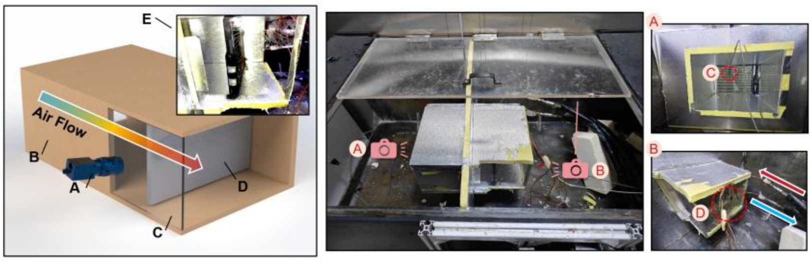

Figure 3: Air duct: schematic diagram (left subfigure, A: industrial CCD camera, B: polyurethane rigid foam sheet, C: transparent acrylic plate, D: the tested condenser, E: photo of the air duct (right subfigure, A: front view of the condenser, B: back view of the condenser, C & D: thermocouples for air temperature measurement).

3. Experimental results and discussion

3.1. Flow Visualization around Different Positioned Orifices.

Figure 4 presents video screenshots of the refrigerant flowing in the headers at a mass flow rate of 0.3 g/s. The top views exhibit a phenomenon of condensate accumulation over the lowest flat tube near the baffle. A shiny stripe is observed on the liquid surface near the liquid-metal contact area (Figure 4, a1.1, b1.1, c1.1). These shiny stripes, indicating a liquid surface with a large and rapidly changing curvature, are also present on the liquid surface when the liquid level is below the flat tubes (Figure 4, b1.2, c1.1). In the tube-side orifice condenser, the liquid level is nearly aligned with the flat tube, and no obvious shiny stripe is observed (Figure 4, a1.2). This indicates that the tube-side orifice condenser has the greatest liquid accumulation among the three condenser types with different orifice positions. In the bottom views of the central-orifice and header-side orifice condensers, condensate flows through the orifices and forms stable liquid columns (Figure 4, b2.1, c2.1). The liquid column in the header-side orifice condenser exhibits intermittent shaking, and the transparent liquid column becomes opaque (Figure 4, c2.2). A small vortex emerges above the orifice (Figure 4, c1.2). Sometimes the end of this liquid column splashes into droplets. The liquid column, however, is absent in the tube-side orifice condenser, as the liquid refrigerant flows out of the orifice intermittently in the form of droplets (Figure 4, a2.2). This indicates that the tube-side orifice has a higher flow resistance than orifices at other positions, which results in more liquid accumulation over the baffle. Another noteworthy phenomenon is that, in the bottom views, the liquid refrigerant flows out of the flat tubes intermittently, varying both over time and across different microchannels.

Figure 5 presents video screenshots of refrigerant flowing in the headers at a mass flow rate of 0.5 g/s. The higher mass flow rate results in different flow characteristics. The most conspicuous difference is that the shiny stripes are highly unstable compared to those at 0.3 g/s (Figure 5, b1.1, b1.2, c1.1). Refrigerant flowing out of the microchannels impinges on the observation window due to its greater inertia (Figure 5, b1.3). This phenomenon occurs in each condenser but is especially pronounced in the central-orifice one. The vortex in the header-side orifice condenser becomes more turbulent, indicating greater gas entrainment through the orifice (Figure 5, c1.2). Nevertheless, the liquid column alternates between transparent and opaque states without splashing, as the flowing liquid features larger inertia force. The liquid column in the central-orifice condenser remains stable and transparent, indicating minimal gas entrainment (Figure 5, b2.1). The liquid level observed in the bottom view of the central-orifice condenser is lower than that observed at 0.3 g/s (Figure 5, b2). The flow pattern in the tube-side orifice condenser differs only slightly from that at the lower mass flow rate (Figure 5, a1). The time interval between dripping droplets decreases, and the droplet size increases (Figure 5, a2).

Quantitative analysis was conducted to compare the liquid levels of central orifice and header-side orifice condensers under different operating conditions. The images were tuned into the same perspective and made semi-transparent before comparison. The comparison results are presented in Figure 6. As the flat tube width is 12 mm, the distance between the liquid level and the flat tube can be calculated proportionally. At the mass flow rate of 0.3 g/s, the distance for the central orifice condenser is 1.65 mm, compared to 1.11 mm for the header-side orifice variant (Figure 6a). The distance of the central orifice condenser was 0.54 mm larger than that of the header-side orifice variant, indicating that the central orifice condenser held a lower liquid level. Therefore, more condensate flows through the orifice in the central orifice condenser and the liquid level below the baffle is higher. At 0.5 g/s, the distances were both 1.08 mm, reflecting enhanced condensation due to a larger heat transfer temperature difference and a stronger heat transfer (Figure 6b).

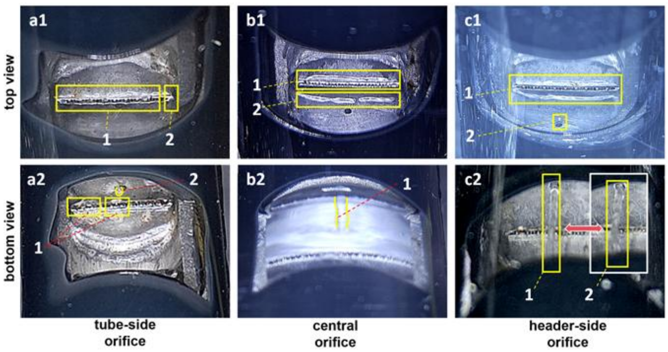

Figure 4: Top and bottom views of refrigerant flow characteristics at 0.3 g/s (channel type: inner-grooved, orifice diameter: 0.6 mm).

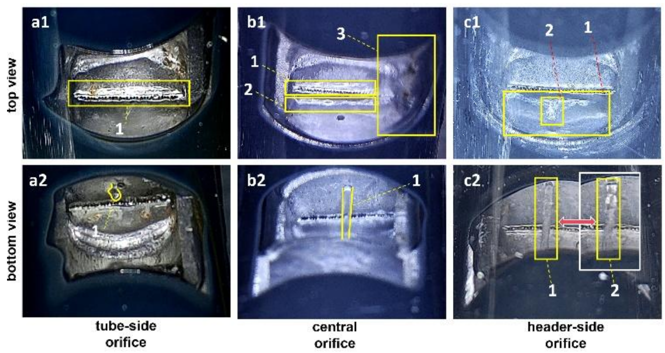

Figure 5: Top and bottom views of refrigerant flow characteristics at 0.5 g/s (channel type: inner-grooved, orifice diameter: 0.6 mm).

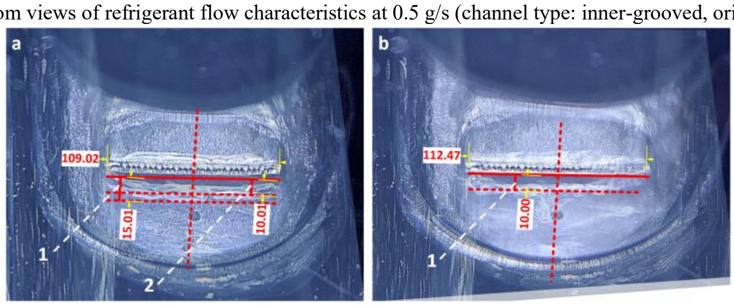

Figure 6: Distances between liquid levels and flat tubes: (a) liquid levels over central and header-side orifice at 0.3 g/s, (b) liquid levels over central and header-side orifice at 0.5 g/s.

3.2. Thermohydraulic Performance of Tested Condensers

Figure 7 presents a comparison of the pressure drop and subcooling degree between the condensers described in Section 3.1 and the baseline condenser without an orifice. All three header-orifice condensers show lower pressure drops (3.2 to 3.3 kPa) than the baseline condenser (3.7 kPa) at a mass flow rate of 0.3 g/s

(Figure 7(a)). This is attributed to a reduction in mass flux in Passes 2 and 3, as a portion of the liquid is diverted through the orifices into the lower header. The measured subcooling degrees are very similar. The maximum deviation between the subcooling degrees is merely 0.19 K (Figure 7(a)). This demonstrates that the increase in refrigerant quality in Passes 2 and 3 compensates for the weakened heat transfer caused by the reduction in mass flux. The results also imply that the liquid-vapor separation performance does not depend strongly on the orifice position when there is adequate condensate accumulated over the orifice. When the mass flow rate was 0.5 g/s, the condensing pressure was adjusted to 590 kPa, resulting in a 2 K increase in the heat transfer temperature difference, to obtain a similar liquid-vapor separation performance as at 0.3 g/s. The pressure drops of the header-orifice condensers (4.0 to 4.1 kPa) are also lower than that of the baseline condenser (4.5 kPa) (Figure 7(b)). All four condensers have similar subcooling degrees as well (Figure 7(b)). The subcooling degrees at 0.5 g/s are about 2 K larger than those at 0.3 g/s, corresponding to the increase in the heat transfer temperature difference. Furthermore, the difference in pressure drop between the header-orifice condensers and the baseline condenser is also similar to that at 0.3 g/s. This suggests that, compared to the case at 0.3 g/s, the refrigerant condenses earlier in Passes 2 and 3, leading to more liquid being diverted through the orifices.

Figure 8 presents a comparison of the pressure drop and subcooling degree between the condensers with smooth tubes and 1.0 mm diameter orifices and the baseline condenser without an orifice. The results illustrate a thermohydraulic performance that differs from that of the inner-grooved variants, due to insufficient liquid accumulation over the orifice baffles. At a mass flow rate of 0.3 g/s, the tube-side orifice condenser exhibits a lower pressure drop (4.1 kPa) than both the central orifice condenser (5.3 kPa) and the baseline condenser (5.2 kPa) (Figure 8(a)). This implies that the tube-side orifice condenser achieves better liquid-vapor separation performance than the central orifice condenser, resulting in less gas entrainment through the orifice. In the central orifice condenser, a considerable amount of gas is entrained and flows through the orifice into Pass 4. Consequently, the advantage of mass flux reduction for reducing pressure drop in Passes 2 and 3 is negated by the increased refrigerant quality in Pass 4. The tested condensers have very similar subcooling degrees (Figure 8(a)), the underlying reasons for which differ depending on the orifice position. In the tube-side orifice condenser, less gas is entrained into Pass 4 through the orifice than in the central orifice condenser. The heat transfer enhancement from the quality increase is offset by the mass flux reduction in Passes 2 and 3. Furthermore, the sufficient heat transfer area in Pass 4 ensures that any entrained gas is completely condensed. As for the central orifice condenser with greater gas entrainment, the entrained gas is also entirely condensed, confirming that the heat transfer area is sufficient. At a mass flow rate of 0.5 g/s, the pressure drops of the baseline, central orifice, and tube-side orifice condensers decrease in that order. The same trend is observed for the subcooling degrees (Figure 8(b)). All subcooling degrees are below 1 K, suggesting insufficient heat transfer. Due to the high void fraction throughout the condensers, the pressure drops in Passes 2 and 3 are the dominant contributor. Under these conditions, when a complete and stable liquid film does not exist on the baffle, increased refrigerant flow rate through the orifice leads to negative effects on both heat transfer and pressure drop, and the extent of these effects is influenced by the orifice position.

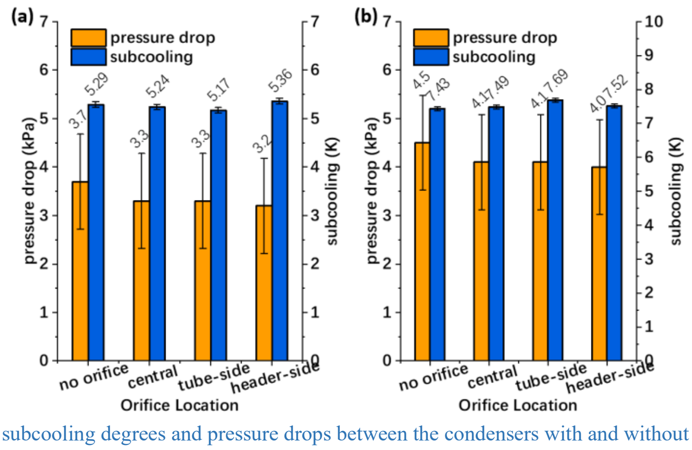

Figure 7: Comparison of subcooling degrees and pressure drops between the condensers with and without orifice. The condensers equipped with inner-grooved microchannel flat tubes and a 0.6 mm diameter orifice. (a) measured at 0.3 g/s, (b) measured at 0.5 g/s. (The coverage factor k is taken as 2.)

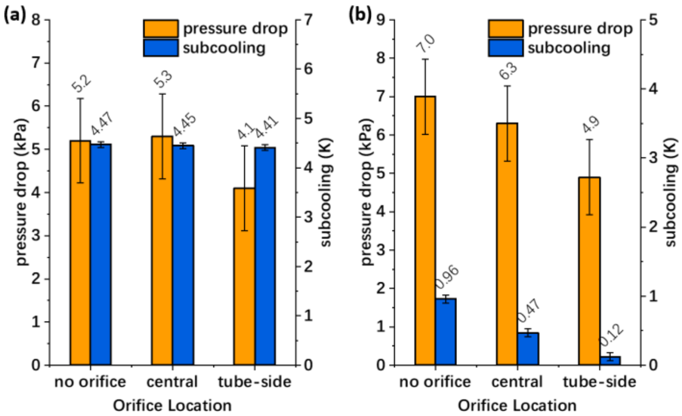

Figure 8: Comparison of subcooling degrees and pressure drops between the condensers with and without orifice. The condensers equipped with smooth microchannel flat tubes and a 1.0 mm diameter orifice. (a) measured at 0.3 g/s, (b) measured at 0.5 g/s. (The coverage factor k is taken as 2.)

3.3. Quantitative results on heat transfer rate increasement of orificed condensers

In this section, the pressure drop data were converted into more intuitive heat transfer rates to better reveal the advantages of the header-orifice structure. By increasing the mass flow rate, the pressure drop of each orificed condenser was adjusted to match that of the baseline (non-orificed) condenser. This approach determined the maximum achievable heat transfer improvement resulting from the pressure drop reduction afforded by the header-orifice design. The heat transfer rates were calculated based on the refrigerant states at the inlet and outlet, while all other boundary conditions remained identical to those in the previous sections. The results are presented in Figure 9. As shown, increasing the mass flow rate led to a decrease in the subcooling degree. This occurred because a greater portion of the heat transfer area was occupied by two-phase refrigerant, leaving insufficient area to further cool the liquid-phase refrigerant down. The orificed condensers exhibited better heat transfer performance at both 0.3 g/s and 0.5 g/s.

At 0.3 g/s, the central orificed condenser achieved the greatest improvement, with a heat transfer rate of 117.0 W. This represented an increase of approximately 12.4% over the baseline value of 104.1 W. This suggested that the central orifice promoted liquid flow while restricting gas flow through the orifice. In contrast, the header-side orifice allowed more gas to pass through, whereas the tube-side orifice reduced liquid flow through the orifice due to a larger capillary force. At 0.5 g/s, the central orificed condenser again achieved the highest heat transfer rate, measuring 183.0 W, with a 9.3% increase over the baseline value of 167.5 W. This finding further supports the conclusion drawn at the lower mass flow rate.

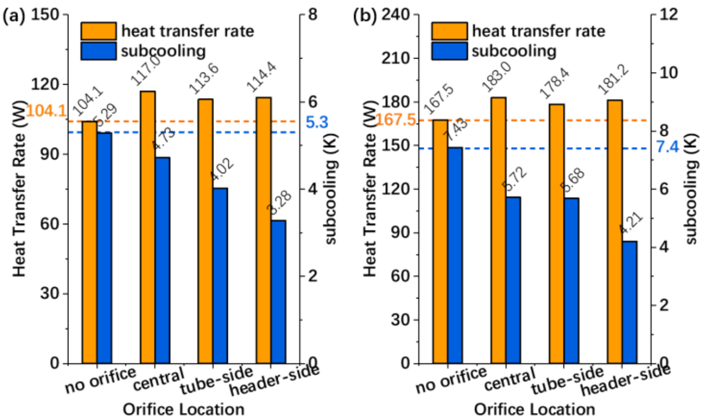

Figure 9: Comparison of heat transfer rate and subcooling degree for orificed condensers under identical pressure drop conditions, relative to the non-orificed baseline. All condensers were equipped with inner-grooved microchannel flat tubes and incorporated a 0.6 mm diameter orifice. Results are shown for two baseline mass flow rates: (a) 0.3 g/s and (b) 0.5 g/s.

4. Conclusion

In this study, two kinds of header-orifice condensers were fabricated and tested in a heat exchanger test rig under ambient conditions of 32°C and 55% relative humidity. R600a was chosen as the working fluid, with a mass flow rate of 0.3 g/s and 0.5 g/s, respectively. Flow visualization and thermohydraulic performance were recorded in the experiment. Comparing and analysing the experimental results, some conclusions were introduced:

1) *Orifice Position and Performance*: The orifice position significantly influenced the condenser performance when the liquid level over the baffle was unstable or insufficient. Under these conditions, the tube-side orifice condenser outperformed the central orifice condenser, achieving pressure drop reductions of 1.1 kPa and 2.1 kPa at 0.3 g/s and 0.5 g/s, respectively. In contrast, the central orifice condenser showed minimal improvements, with reductions of -0.1 kPa and 0.7 kPa under the same conditions.

2) *Stable Liquid Level*: When a stable and thick liquid level was maintained over an orifice, the orifice position had a minimal influence on condenser performance. In such cases, the tube-side and central orifice condensers both achieved pressure drop reductions of 0.4 kPa at 0.3 g/s and 0.5 g/s, while the header-side orifice condenser achieved reductions of 0.5 kPa under the same conditions.

3) *Liquid Accumulation and Surface Tension*: When it was challenging to establishing a stable and thick liquid level over the orifice, the tube-side orifice position is likely to accumulate liquid easier due to surface tension. However, when liquid was adequate (e.g., with strong heat transfer or a small orifice diameter), the orifice position had little effect.

4) *Liquid Level Distance*: Shiny stripes on the liquid surface imply the lowest are of the accumulated condensate. The distance between liquid level and flat tube can be calculated using the photograph from CCD camera. At a mass flow rate of 0.3 g/s, the distances for the central orifice and header-side orifice were 1.65 mm and 1.11 mm, respectively. At a mass flow rate of 0.5 g/s, both the distances decreased to 1.08 mm, with the header-side orifice exhibiting vortex formation. The order of liquid accumulation ease at 0.3 g/s was: tube-side orifice > central orifice > header-side orifice. At 0.5 g/s, the order simplified to: tube-side orifice > other orifice types.

5) *Quantitative results on heat transfer rate increasement*: A quantitative comparison was conducted to evaluate the heat transfer enhancement of condensers with an orifice against the non-orificed baseline, under identical pressure drop conditions. The central orificed condenser demonstrated the best performance among all orificed configurations. Specifically, it achieved heat transfer rate increases of 12.4% and 9.3% relative to the baseline at the two tested conditions, respectively. This result indicates that the central orificed design excels when sufficient liquid is present above the orifice. Conversely, the tube-side orifice may be the preferable choice in scenarios where liquid accumulation is difficult.

Acknowledgements

This study was supported by Hisense Refrigerator Co. Ltd.

References

[1] S. A. E. Sayed Ahmed, O. M. Mesalhy, and M. A. Abdelatief, “Flow and heat transfer enhancement in tube heat exchangers,” *Heat Mass Transf.*, vol. 51, no. 11, pp. 1607–1630, Nov. 2015, doi: 10.1007/s00231-015-1669-1.

[2] K. Oh, S. Lee, T. Park, and Y. Kim, “Multistage gas and liquid phase separation condenser,” Aug. 03, 2004

[3] J. Li and P. Hrnjak, “Phase Separation in Second Header of MAC Condenser,” presented at the SAE 2015 World Congress & Exhibition, Apr. 2015, pp. 2015-01–1694. doi: 10.4271/2015-01-1694.

[4] J. Li and P. Hrnjak, “Improvement of condenser performance by phase separation confirmed experimentally and by modeling,” *Int. J. Refrig.*, vol. 78, pp. 60–69, June 2017, doi: 10.1016/j.ijrefrig.2017.03.018.

[5] J. Li and P. Hrnjak, “Visualization and quantification of separation of liquid-vapor two-phase flow in a vertical header at low inlet quality,” *Int. J. Refrig.*, vol. 85, pp. 144–156, Jan. 2018, doi: 10.1016/j.ijrefrig.2017.09.018.

[6] D. Wu, Z. Wang, G. Lu, and X. Peng, “High-Performance Air Cooling Condenser With Liquid–Vapor Separation,” *Heat Transf. Eng.*, vol. 31, no. 12, pp. 973–980, Oct. 2010, doi: 10.1080/01457631003638952.

[7] Y. Chen, N. Hua, and L. S. Deng, “Performances of a split-type air conditioner employing a condenser with liquid–vapor separation baffles,” *Int. J. Refrig.*, vol. 35, no. 2, pp. 278–289, Mar. 2012, doi: 10.1016/j.ijrefrig.2011.10.014.

[8] X. Chen, Y. Chen, L. Deng, S. Mo, and H. Zhang, “Experimental verification of a condenser with liquid–vapor separation in an air conditioning system,” *Appl. Therm. Eng.*, vol. 51, no. 1–2, pp. 48–54,

Mar. 2013, doi: 10.1016/j.applthermaleng.2012.09.006.
[9] T. M. Zhong *et al.*, “Experimental investigation on microchannel condensers with and without liquid–vapor separation headers,” *Appl. Therm. Eng.*, vol. 73, no. 2, pp. 1510–1518, Dec. 2014, doi: 10.1016/j.applthermaleng.2014.08.047.
[10] J. Chen *et al.*, “Application of a vapor–liquid separation heat exchanger to the air conditioning system at cooling and heating modes,” *Int. J. Refrig.*, vol. 100, pp. 27–36, Apr. 2019, doi: 10.1016/j.ijrefrig.2018.10.030.
[11] X. Luo *et al.*, “Thermo-economic analysis and optimization of a zoetropic fluid organic Rankine cycle with liquid-vapor separation during condensation,” *Energy Convers. Manag.*, vol. 148, pp. 517–532, Sept. 2017, doi: 10.1016/j.enconman.2017.06.002.
[12] N. Conte, “The Top Retailers in the World, by Store Count,” Visual Capitalist. Accessed: Nov. 13, 2025. [Online]. Available: https://www.visualcapitalist.com/top-retailers-in-the-world-by-store-count/